Porous Amorphous Metal-organic Frameworks based on Heterotopic Triangular Ligands for Iodine and High-Capacity Dye Adsorption

Ying Feng,[a] Liang-Hua Wu,[a] Chu-Hong Zhang,[a] Bing-Xun Zhou,[a] Sheng-Run Zheng*[a], Wei-Guang Zhang*[a], Song-Liang Cai,[a] and Jun Fan[ab]

[a]GDMPA Key Laboratory for Process Control and Quality Evaluation of Chiral Pharmaceuticals, And Guangzhou Key Laboratory of Analytical Chemistry for Biomedicine, School of Chemistry, South China Normal University, Guangzhou 510006, China.

[b]MOE Key Laboratory of Laser Life Science & Institute of Laser Life Science, Guangdong Provincial Key Laboratory of Laser Life Science, College of Biophotonics, South China Normal University, Guangzhou 510631, China.

*Corresponding author: Dr. Sheng-Run, Zheng; Dr. Wei-Guang Zhang

E-mail address: zhengsr@scnu.edu.cn; wgzhang@scnu.edu.cn

Tel./Fax.: +86-20-39310187

Supporting Information

EXAFX Analysis

Data reduction, data analysis, and EXAFS fitting were performed and analyzed with the Athena and Artemis programs of the Demeter data analysis packages[1] that utilizes the FEFF6 program[2] to fit the EXAFS data. The energy calibration of the sample was conducted through a standard Co foil, which as a reference was simultaneously measured. A linear function was subtracted from the pre-edge region, then the edge jump was normalized using Athena software. The χ(k) data were isolated by subtracting a smooth, three-stage polynomial approximating the absorption background of an isolated atom. The k3-weighted χ(k) data were Fourier transformed after applying a Hanning window function (Δk = 1.0). For EXAFS modeling, the global amplitude EXAFS (*CN, R,* σ^2 and ΔE_0) were obtained by nonlinear fitting, with least-

squares refinement, of the EXAFS equation to the Fourier-transformed data in R-space, using Artemis software, EXAFS of the Co foil is fitted and the obtained amplitude reduction factor S_0^2 value (0.802) was set in the EXAFS analysis to determine the coordination numbers (CNs) in the Co-N/O/Co scattering path in sample.

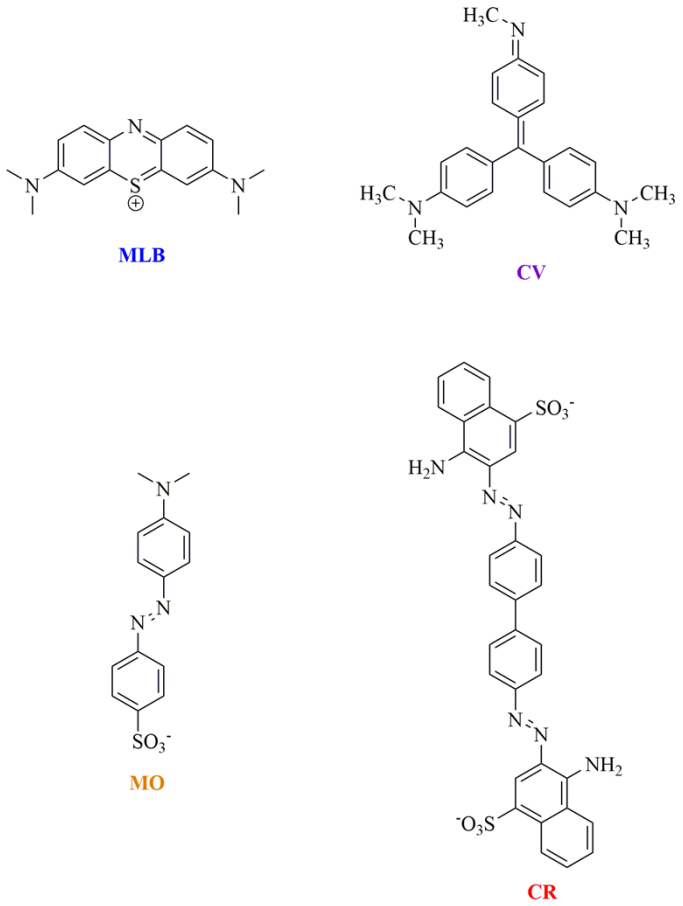

Fig. S1 The structures of the selected dye molecules

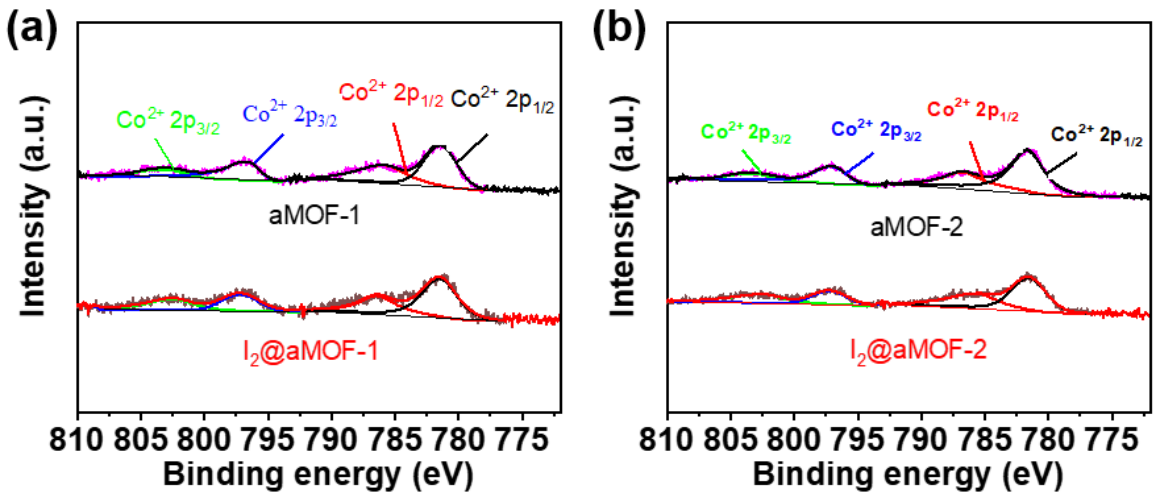

Fig. S2 (a) Co 2p XPS of aMOF-1 and I_2@aMOF-1. (b) Co 2p XPS of aMOF-2 and I_2@aMOF-2.

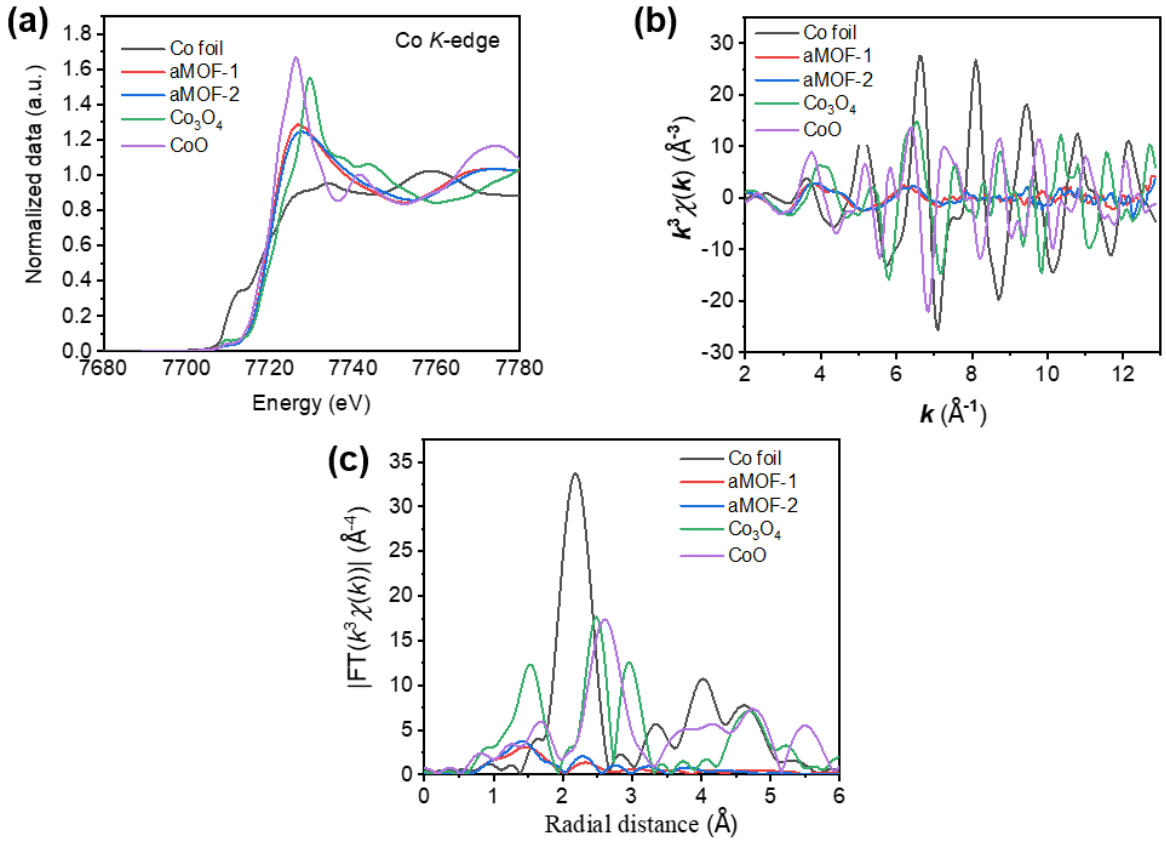

Fig. S3 (a) K-edge XANES spectra of aMOF-1, aMOF-2 and reference samples of CoO and Co foil. Fourier transform extended X-ray absorption structure spectra at the Co K-edge of aMOF-1, aMOF-2 and reference samples of CoO and Co foil at the (b) K(e) and (c) R(f) spaces.

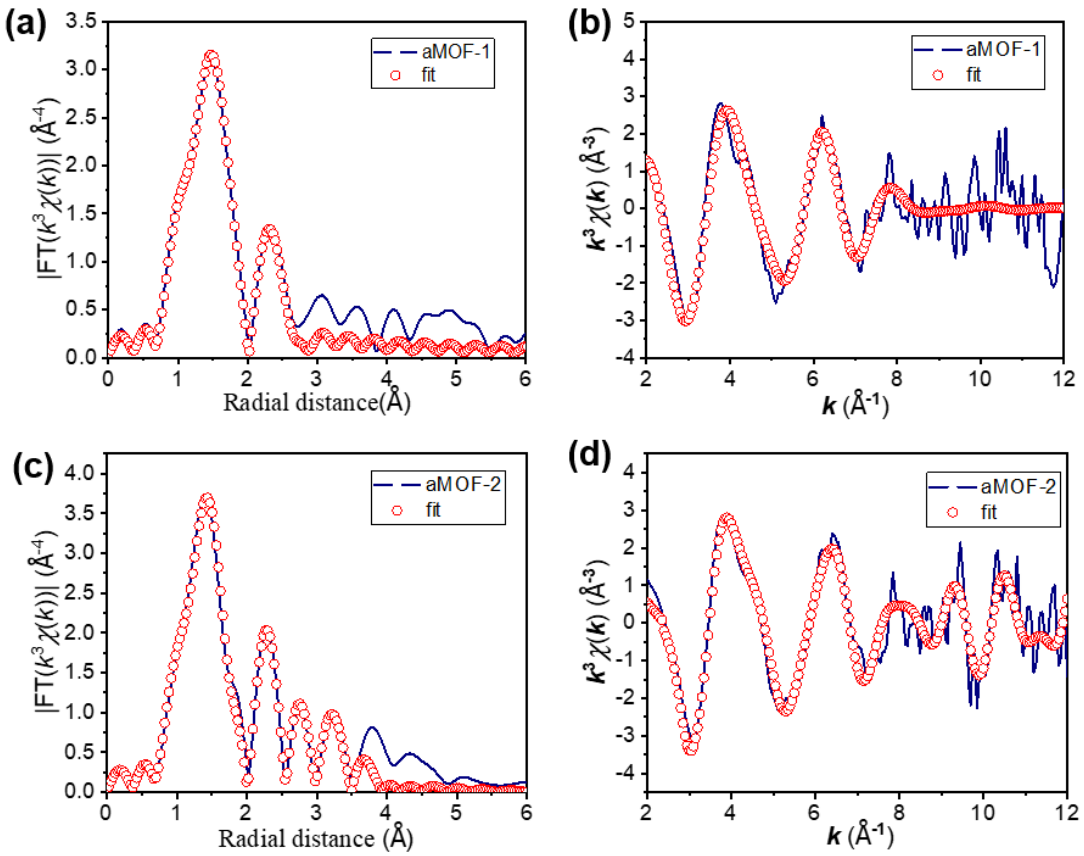

Fig. S4 EXAFS fitting results of FT-EXAFX spectra at the Co K-edge of (a) aMOF-1 and (c) aMOF-2 at the R(f) spaces, and (b) aMOF-1 and (d) aMOF-2 at the K(e) spaces.

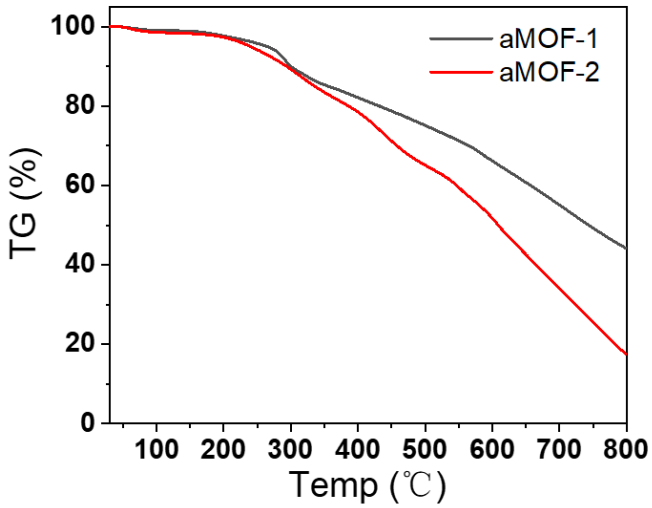

Fig. S5 TG curve of aMOF-1 and aMOF-2.

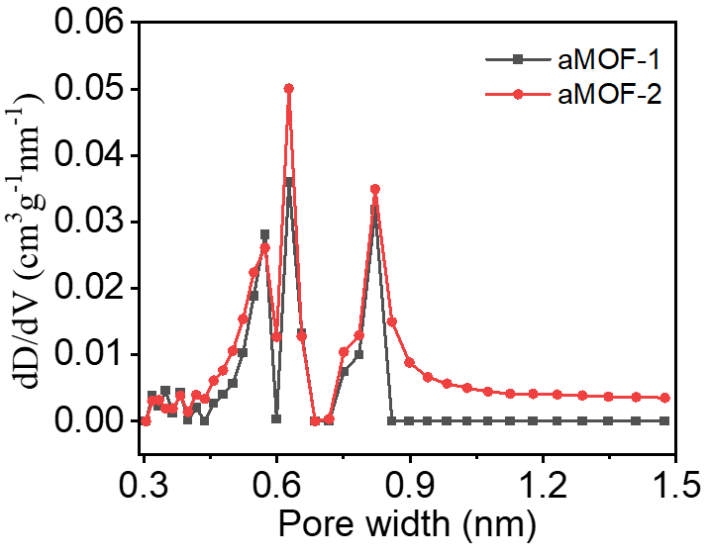

Fig. S6 Pore size distribution simulation of CO_2 adsorption for aMOF-1 and aMOF-2 at 273 K.

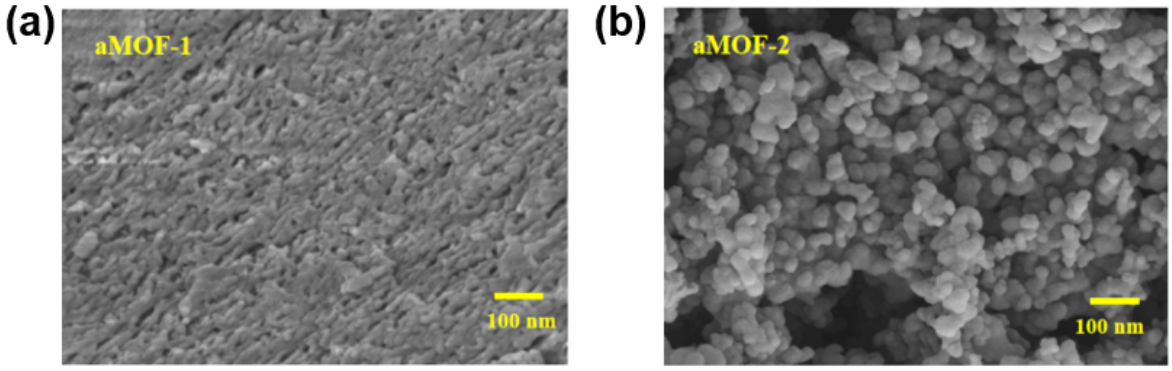

Fig. S7 SEM of (a) aMOF-1 and (b) aMOF-2.

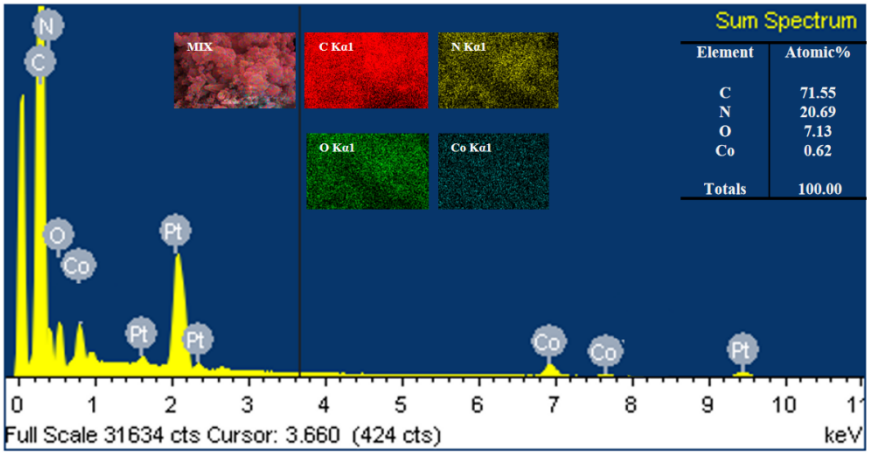

Fig. S8 EDS spectra of aMOF-1.

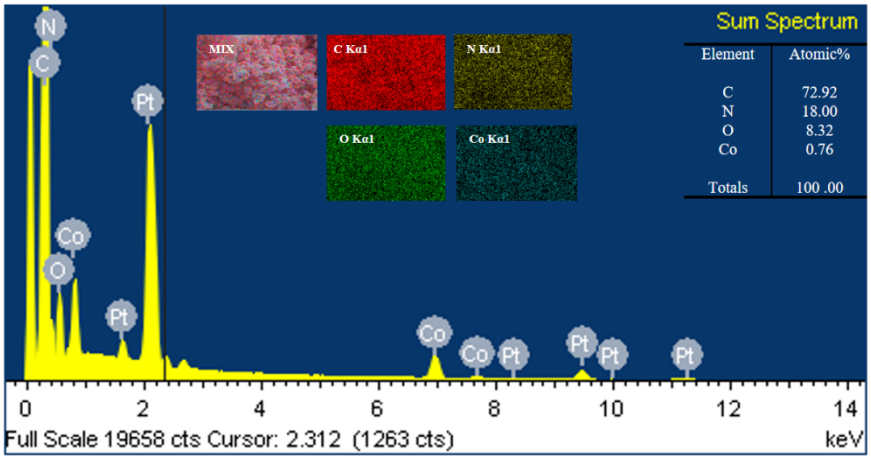

Fig. S9 EDS spectra of aMOF-2.

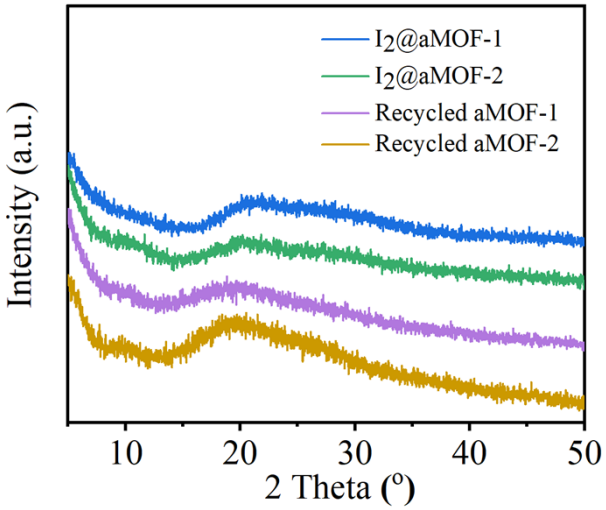

Fig. S10 PXRD of I_2@aMOF-1, I_2@aMOF-2, recycled aMOF-1, and recycled aMOF-2.

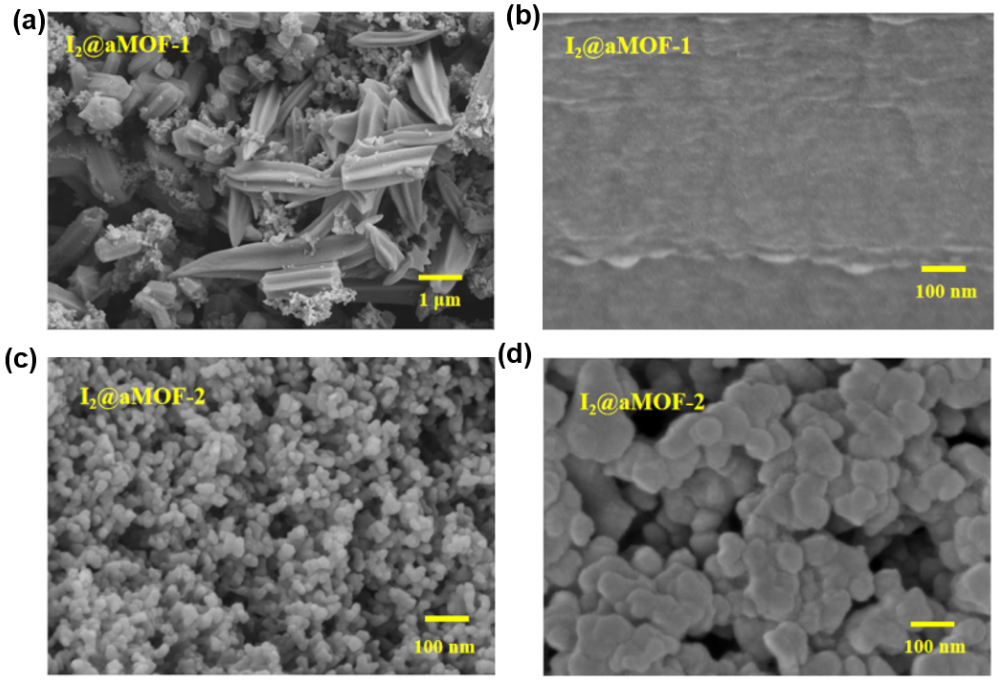

Fig. S11 SEM of I_2@aMOF-1(a and b) and I_2@aMOF-2 (c and d).

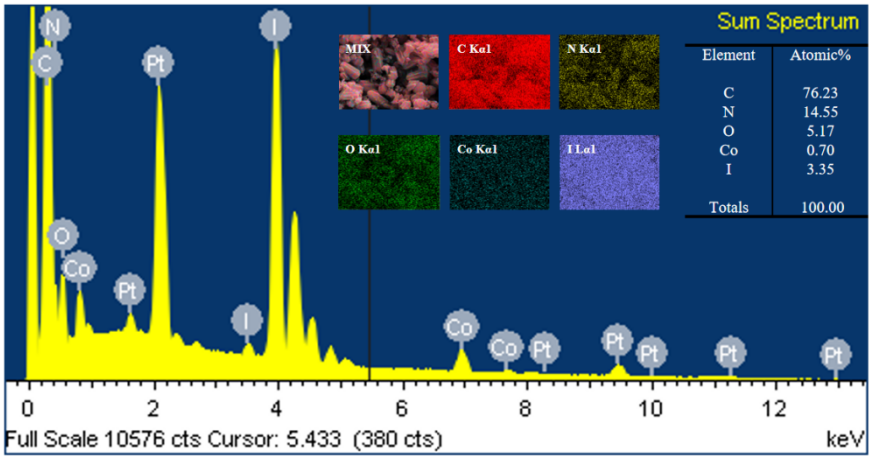

Fig. S12 EDS spectra of I_2@aMOF-1.

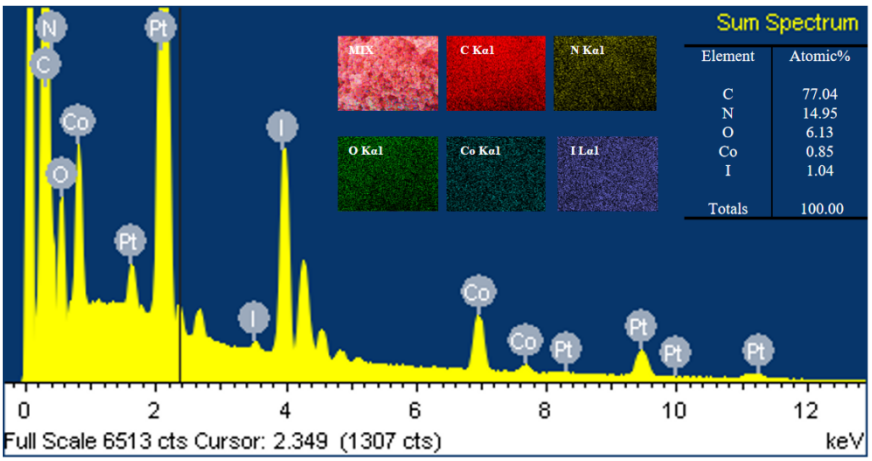

Fig. S13 EDS spectra of I_2@aMOF-2.

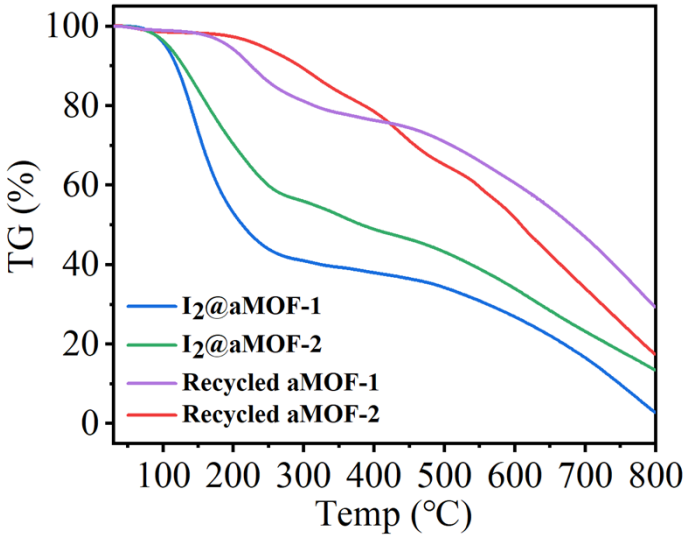

Fig. S14 TG curve of I_2@aMOF-1, I_2@aMOF-2, recycled aMOF-1, and recycled aMOF-2.

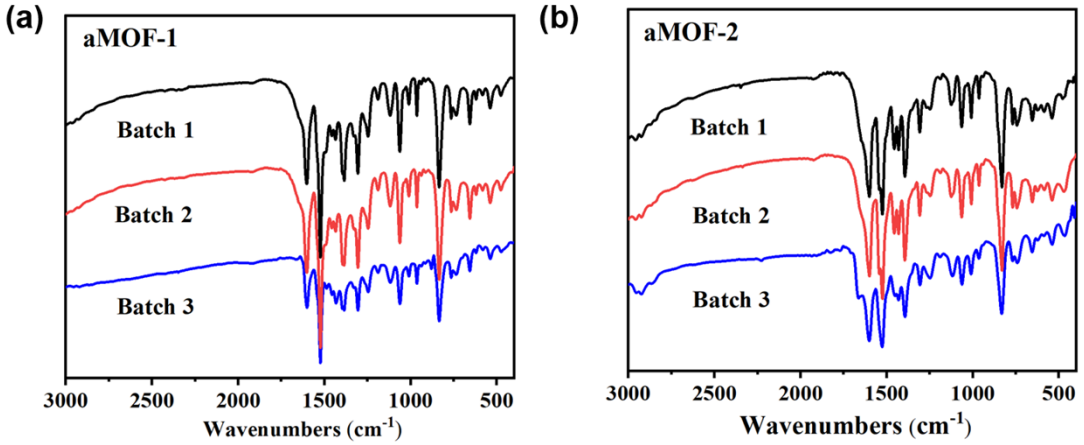

Fig. S15 Infrared spectra of (a) aMOF-1 and (b) aMOF-2 from different batches.

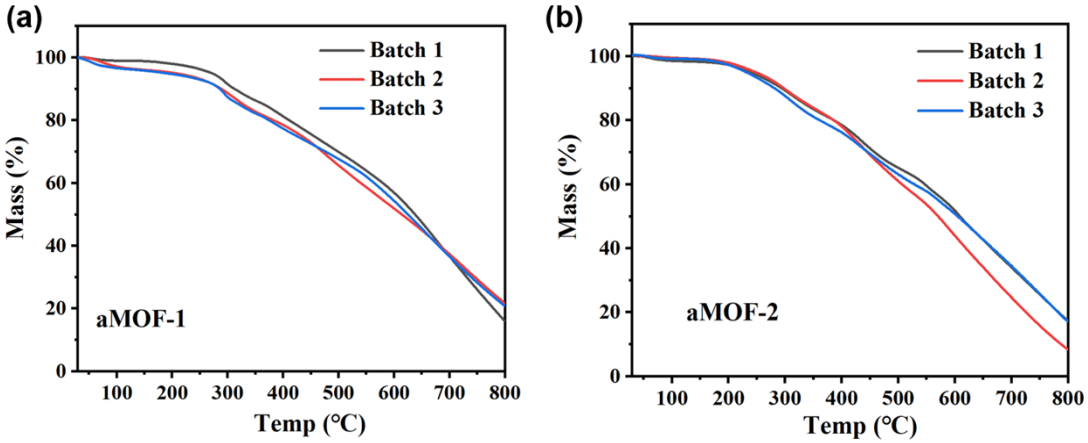

Fig. S16 TG curves of (a) aMOF-1 and (b) aMOF-2 from different batches.

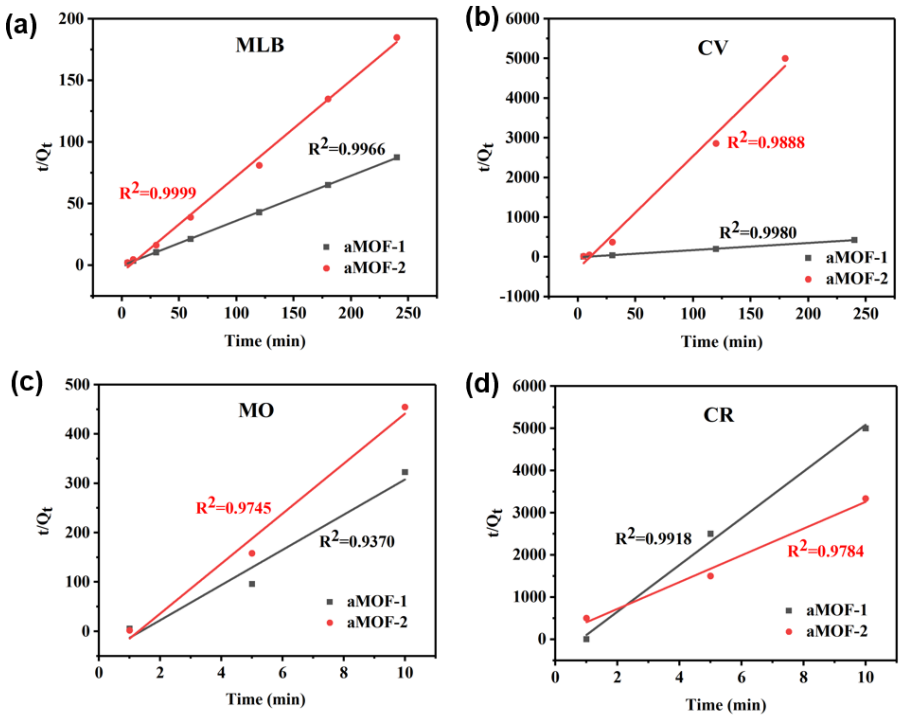

Fig. S17 Plot of the pseudo-second order kinetic model for MLB (a), CV (b), MO (c) and CR (d) on aMOF-1(a and b) and I_2@aMOF-2.

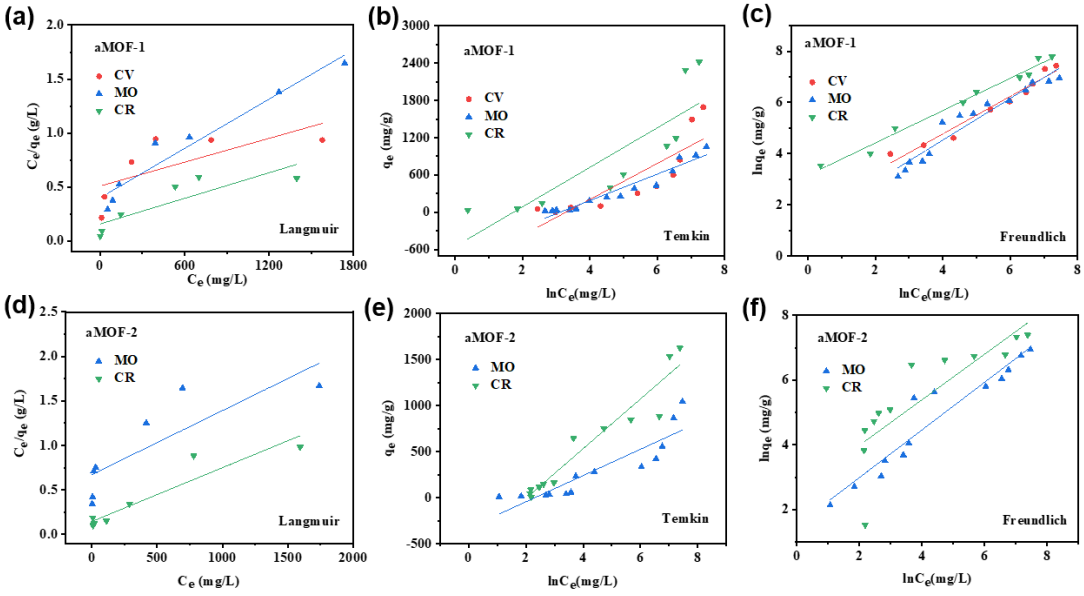

Fig. S18 Plots of the fitting of the dye adsorption experimental data on aMOF-1 with (a) Langmuir isotherm, (b) Themkin and (c) Freundlich isotherm models. Plots of the fitting of the dye adsorption experimental data on aMOF-2 with (d) Langmuir isotherm, (e) Themkin and (f) Freundlich isotherm models.

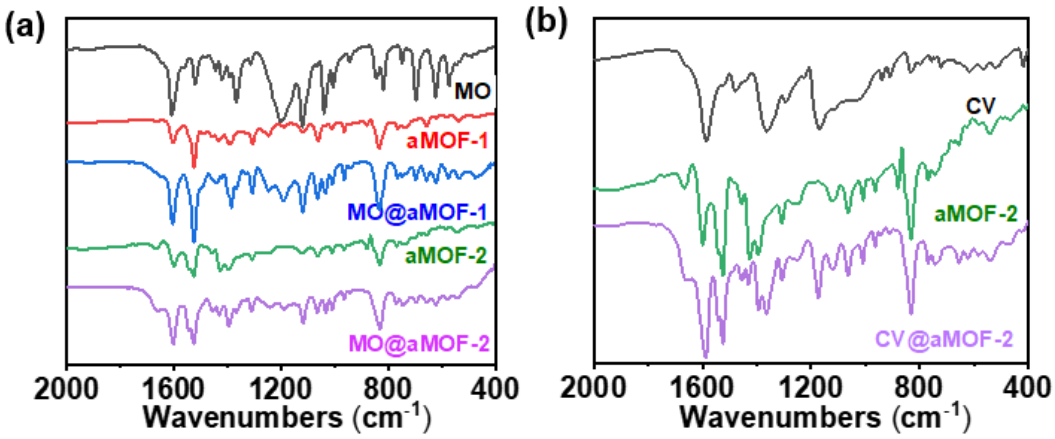

Fig. S19 (a) IR spectra of aMOF-1 and aMOF-2 before and after MO adsorption. (b) IR spectra of aMOF-2 before and after CV adsorption.

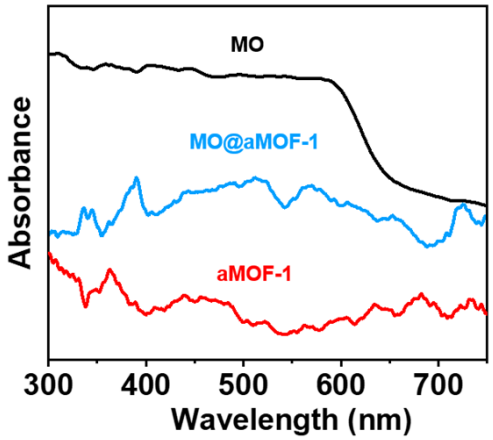

Fig. S20 Solid-state UV-Vis spectra of MO, aMOF-1 and MO@aMOF-1.

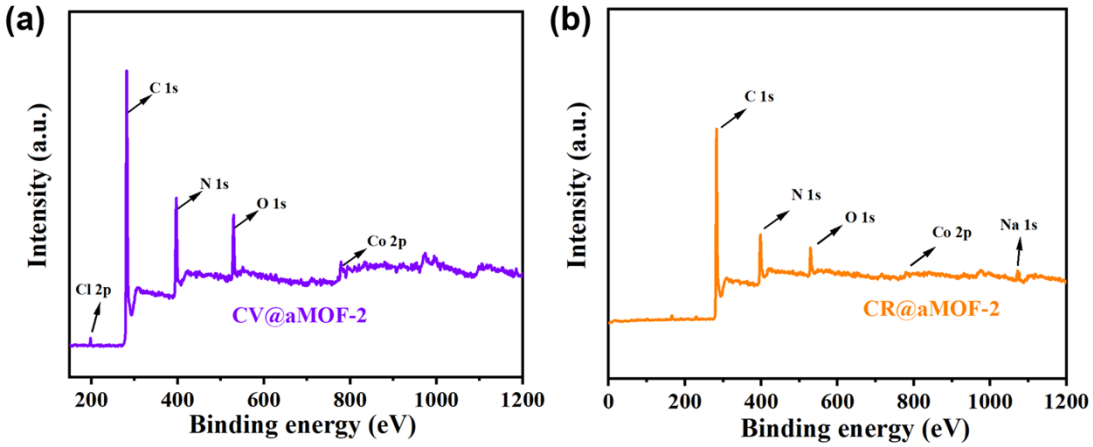

Fig. S21 XPS full spectra of (a) CV@aMOF-2 and (a) CR@aMOF-2.

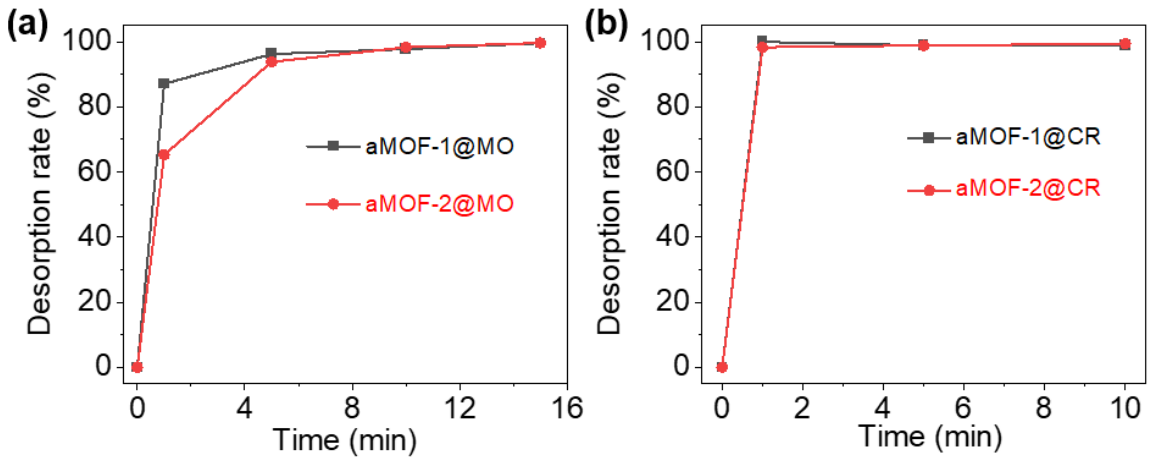

Fig. S22 (a) The desorption rate of MO@aMOF-1 and MO@aMOF-2. (b) The desorption rate of CR@aMOF-1 and CR@aMOF-2.

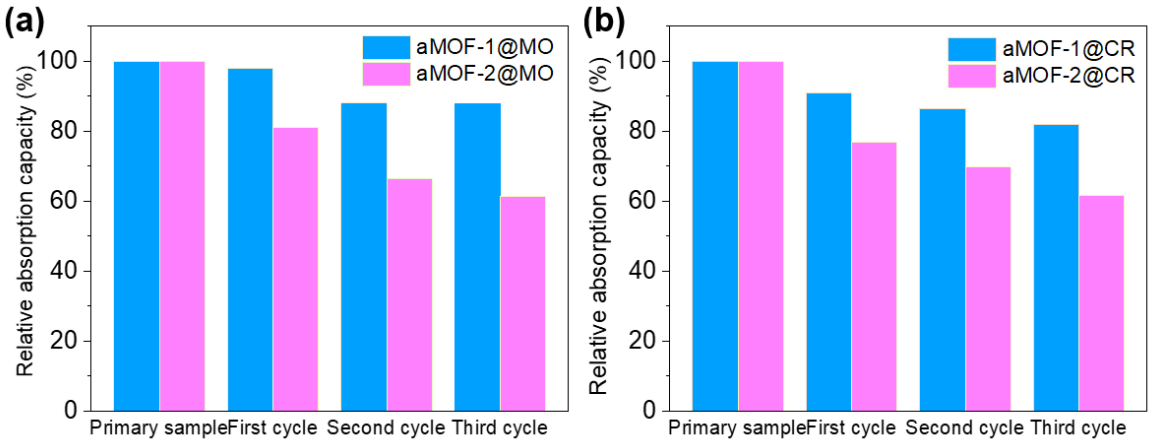

Fig. S23 (a) The recycle test of aMOF-1 and aMOF-2 on MO adsorption. (b) The recycle test of aMOF-1 and aMOF-2 on CR adsorption.

Table S1. Comparisons of the absorbance of the dye solutions (20 ppm, 2 mL) after adding amorphous solids (2 mg) obtained from different synthesized conditions for 30 min.

		HBITP		H_2IBTP	
		MO	MLB	MO	MLB
$Co(NO_3)\cdot 6H_2O$	Acidic (By adding HNO_3)	0.87	2.92	0.62	1.93
	Neutral	0.12	2.83	0.035	1.67
	Alkaline (By adding $NH_3\cdot H_2O$)	0.070	2.73	0.023	1.02
$Ni(NO_3)\cdot 6H_2O$	Acidic (By adding HNO_3)	0.53	2.85	0.72	2.31
	Neutral	0.20	2.73	0.052	1.89
	Alkaline (By adding $NH_3\cdot H_2O$)	0.10	2.69	0.044	1.11

Table S2. EXAFS fitting parameters at the Co *K*-edge for various samples （S_0^2=0.813）

Sample	Shell	*CN*[a]	*R*(Å)[b]	σ^2(Å^2)[c]	ΔE_0(eV)[d]	*R* factor
aMOF-1	Co-N	5.8±0.3	2.033±0.021	0.0058±0.0036	-1.4±1.9	0.0066
aMOF-2	Co-N	6.2±0.1	1.932±0.023	0.049±0.0037	6.5±1.6	0.0053
	Co-Co	1.2±0.1	3.039±0.011	0.0145±0.0093		
	Co-Co	1.3±0.3	3.700±0.016			

[a]*CN*, coordination number; [b]*R*, the distance to the neighboring atom; [c]σ^2, the Mean Square Relative Displacement (MSRD); [d]ΔE_0, inner potential correction; *R* factor indicates the goodness of the fit. $S0^2$ was fixed to 0.813, according to the experimental EXAFS fit of Co foil by fixing *CN* as the known crystallographic value. * This value was fixed during EXAFS fitting, based on the known structure of Co. Fitting range: $3.0 \le k$ (/Å) ≤ 12.5 and $1.0 \le R$ (Å) ≤ 3.0 (Co foil); $1.0 \le k$ (/Å) ≤ 10.2 and $1.0 \le R$ (Å) ≤ 3.0 (Co1); $2.0 \le k$ (/Å) ≤ 12.2 and $1.0 \le R$ (Å) ≤ 4.5 (Co2). A reasonable range of EXAFS fitting parameters: $0.700 < S_0^2 < 1.000$; $CN > 0$; $\sigma^2 > 0$ Å^2; $|\Delta E_0| < 10$ eV; *R* factor < 0.02.

Table S3 The mesopore porosity analysis for aMOFs

Sample	[a]S_{BET} (m^2/g)	[b]V_{meso} (cm^3/g)	[c]V_{micro} (cm^3/g)	[b]V_{meso}/[c]V_{micro}	[d]D_{NLDFT} (nm)
aMOF-1	39.31	0.25	0.053	4.72	1.7~31.5
aMOF-2	136.26	0.15	0.18	0.83	0.6~2.0

[a]S_{BET} is the BET-specific surface area.
[b]V_{meso} is the specific mesopore volume obtained from the BJH cumulative specific desorption volume of pores of 1.70 to 300.00 nm in diameter.
[c]V_{micro} is the t-diagram method of micropore volume.
[d]D_{NLDFT} is the pore size distribution based on the NLDFT model.

Table S4 The comparisons of adsorption capacities on iodine and dye uptake aMOF-1 and aMOF-2.

Samples	Iodine uptake capacity (g/g)	Dye uptake capacity (g/g)			
		MLB	CV	MO	CR
aMOF-1	3.30	----	----	0.921	2.417
aMOF-2	0.56	----	1079	1042	1625

Table S5 The measured density of aMOF-1 and aMOF-2 before and after iodine adsorption

Sample	aMOF-1	aMOF-2	I_2@aMOF-1	I_2@aMOF-2
density	1.3026±0.0059	1.2985±0.0032	2.1850±0.0017	1.8493±0.0068

Table S6 The Co content in aMOF-1 and aMOF-2 calculated from ICP results from different batches.

	aMOF-1			aMOF-2		
	Batch 1	Batch 2	Batch 3	Batch 1	Batch 2	Batch 3
Co content (%)	5.74	5.70	5.64	7.99	7.85	8.02

Table S7. Comparisons of the maximum adsorption capacities on MO by selected MOFs

Adsorbents for MO	Adsorption capacity (mg/g)	Ref
MIL-100 (Fe)	1045	[3]
aMOF-2	1042	This work
aMOF-1	921	This work
NDA88-Cu	399	[4]
SCNU-Z1-Cl	285	[5]
MIL-100 (Cr)	212	[6]
MIL-53 (Al)	183	[7]
MIL-53 (Cr)	58	[8]
ZIF-8	2	[9]

Table S8. Comparisons of the maximum adsorption capacities on CR by selected MOFs

Adsorbents for CR	Adsorption capacity (mg/g)	Ref
GO/Ni-MOFs	2489	[10]
aMOF-1	2417	This work
aMOF-2	1625	This work
SCNU-Z4	1200	[11]
Ni/Cu-BTC	1100	[12]
$[Ag_4(dpe)_4]\cdot(butca)\cdot 13H_2O$	739	[13]
SCNU-Z1-Cl	585	[5]
RGO/NH_2-MIL-68 (Al)	474	[14]
$[Cd_2(oba)_2(4\text{-}bpdb)_2]n(DMF)_x$	97	[15]

Reference

S1 B. Ravel and M. Newville, *J Synchrotron Radiat.*, 2005, **12**, 537-541.

S2 S. I. Zabinsky, J. J. Rehr, A. Ankudinov, R. C. Albers and M. J. Eller, *Phys. Rev. B.*, 1995, **52**, 2995-3009.

S3 O. M. Yaghi, M. O'keeffe, N. W. Ockwig, H. K. Chae, M. Eddaoudi and J. Kim, *Nature*, 2003, **423**, 705-714.

S4 J. C. Shen, X. Z. Wang, L. M. Zhang, Z. Yang, W. B. Yang, Z. Q. Tian, J. Q. Chen and T. Tao,

J. Clean. Prod., 2018, **184**, 949-958.
S5 S. Q. Deng, X. J. Mo, S. R. Zheng, X. Jin, Y. Gao, S. L. Cai, J. Fan and W. G Zhang, *Inorg. Chem.*, 2019, **58**, 2899-2909.
S6 M. Tong, D. Liu, Q. Yang, S. Devautour-Vinot, G. Maurin and C. Zhong, *J. Mater. Chem. A*., 2013, **1**, 8534-8537.
S7 M. Al Sharabati and R. Sabouni, *Polyhedron*, 2020, **190**, 114762.
S8 E. Haque, J. E. Lee, I. T. Jang, Y. K. Hwang, J.-S. Chang, J. Jegal and S. H. Jhung, *J. Hazard. Mater*., 2010, **181**, 535-542.
S9 Y. Li, K. Zhou, M. He and J. Yao, *Microporous Mesoporous Mater*., 2016, **234**, 287-292.
S10 S. Zhao, D. Chen, F. Wei, N. Chen, Z. Liang and Y. Luo, *Ultrason. Sonochem*., 2017, **39**, 845-852.
S11 G. Q. Wang, J. F. Huang, X.F. Huang, S. Q. Deng, S. R. Zheng, S. L. Cai, J. Fan and W. G. Zhang, *Inorg. Chem. Front*., 2021, **8**, 1083-1092.
S12 J. Hu, H. Yu, W. Dai, X. Yan, X. Hu and H. Huang, *RSC Adv*., 2014, **4**, 35124-35130.
S13 J. Zhang, C.C. Wang, P. Wang and Y. L. Cao, *RSC Adv*., 2016, **6**, 73595-73599.
S14 Z. Wu, X. Yuan, H. Zhong, H. Wang, L. Jiang, G. Zeng, H. Wang, Z. Liu and Y. Li, *J. Mol. Liq*., 2017, **247**, 215-229
S15 M. Y. Masoomi, A. Morsali and P. C. Junk, *CrystEngComm.*, 2015, **17**, 686-692.